

Cubic Form of $\text{Pb}_{2-x}\text{Sn}_x\text{S}_2$ Stabilized through Size Reduction to the Nanoscale

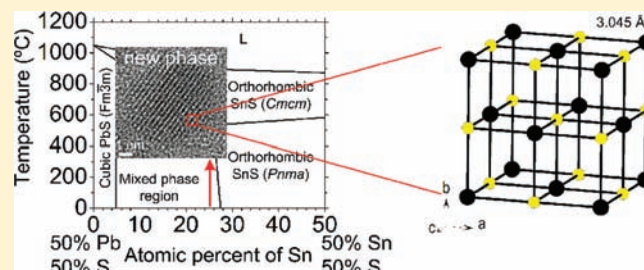
Ronald B. Soriano,[†] Christos D. Malliakas,[†] Jinsong Wu,[‡] and Mercouri G. Kanatzidis^{*,†}

[†]Department of Chemistry, Northwestern University, Evanston, Illinois 60208, United States

[‡]Department of Material Science and Engineering, Northwestern University, Evanston, Illinois 60208, United States

S Supporting Information

ABSTRACT: We demonstrate the synthesis of semiconductor $\text{Pb}_{2-x}\text{Sn}_x\text{S}_2$ nanocrystals with a cubic rock salt crystal structure in a composition range where this structure is unstable in the bulk. The cubic $\text{Pb}_{2-x}\text{Sn}_x\text{S}_2$ nanocrystals were prepared using a modified hot injection colloidal synthetic route. The x value is in the range $0.40 < x < 1$. Even though these compositions lie in a region of the PbS–SnS phase diagram where no single phase exists, and despite the fact that PbSnS_2 is a distorted orthorhombic phase, the $\text{Pb}_{2-x}\text{Sn}_x\text{S}_2$ nanocrystals are single phase solid solutions with cubic NaCl-type structure. Experimental evidence for this derives from powder X-ray diffraction (PXRD), electron diffraction, and pair distribution function (PDF) analysis. Elemental compositions determined using scanning transmission electron microscopy/energy dispersive spectroscopy (STEM/EDS), inductively coupled plasma-atomic emission spectroscopy (ICP-AES), and electron energy loss spectroscopy (EELS) reveal a composition close to the nominal ones. The band gaps of the $\text{Pb}_{2-x}\text{Sn}_x\text{S}_2$ nanocrystals (0.52–0.57 eV) are blue-shifted by quantum confinement relative to that of the hypothetical cubic PbSnS_2 phase which density functional theory (DFT) calculations show to be much narrower (0.2 eV) than in the case of orthorhombic PbSnS_2 (1.1 eV). The $\text{Pb}_{2-x}\text{Sn}_x\text{S}_2$ nanocrystals exhibit a well-defined band gap in the near-IR region and are stable up to ~ 300 °C above which they phase separate into cubic PbS and orthorhombic α -SnS.



INTRODUCTION

PbS and SnS belong to the IV–VI family of semiconducting materials but are not isostructural. They have narrow to medium band gaps (PbS: 0.37 eV, and SnS: 1.3 eV) making them promising for photovoltaic, infrared detection, and thermoelectric applications as well as high-output-power pn-junction lasers and telecommunication relays.^{1–8} These materials also exhibit the ability to generate more than one electron–hole pair per photon absorbed, also known as multiple exciton generation (MEG),^{3,9–11} with positive implications toward the development of highly efficient solar cells. Surprisingly, the ternary semiconductor PbSnS_2 (*teallite*) is only rarely described in the literature. Lead tin sulfide thin films show a high absorption coefficient ($>10^4 \text{ cm}^{-1}$) in the visible range^{12,13} which suggests the PbSnS_2 compound warrants a closer investigation of its properties.

Unlike the heavier chalcogenide rock salt analogs where solid solutions exist of $\text{Pb}_{1-x}\text{Sn}_x\text{Q}$ ($\text{Q} = \text{Se}, \text{Te}$) over the entire range of x , PbSnS_2 appears to be a distinct compound and can be regarded as an end member of the so-called SnS (*herzenbergite*) mineral series of the orthorhombic space group *Pnma*.¹⁴ The lattice parameters of PbSnS_2 are $a = 11.17 \text{ \AA}$, $b = 3.99 \text{ \AA}$, and $c = 4.20 \text{ \AA}$.¹⁴ The mutual $\text{Pb}^{2+}/\text{Sn}^{2+}$ substitution in the structure of sulfides and sulfosalts is known to occur naturally in minerals, and orthorhombic PbSnS_2 is a particular example.¹⁵ Very few studies have been reported on the preparation of bulk

PbSnS_2 or thin films.^{12,13,16} Polymorphism of PbSnS_2 from the orthorhombic *Pnma* space group to the cubic *Fm3m* space group was reported by growing a single crystalline thin film epitaxially onto a freshly cleaved rock salt substrate maintained at 50 °C; however, no evidence for this was provided.¹⁶ The corresponding cubic structure can be thought of as the undistorted or dilated version of the more dense orthorhombic structure (Figure 1).

The phase diagram of the PbS–SnS system reveals a narrow range of solubility between the two end members, Figure 2. Based on this, the limiting solubility of SnS in the rock salt PbS phase is only 10 mol %, and that of PbS in the orthorhombic SnS is about 50 mol %.¹⁷ Between these two concentrations there is no solubility and both the cubic rock salt and the orthorhombic phases exist. Based on this phase diagram of the bulk materials the purpose of this work was to prepare nanocrystals of orthorhombic PbSnS_2 . To our surprise we observe that the nanocrystals we obtain are in a composition range of $\text{Pb}_{2-x}\text{Sn}_x\text{S}_2$ (including $x \approx 1$) that lies well into the thermodynamically stable orthorhombic phase region (Figure 2), but they adopt the rock salt structure type. We show here that, in the nanocrystalline state, the NaCl rock salt structure of $\text{Pb}_{2-x}\text{Sn}_x\text{S}_2$ is stable in the range $0.60 < x < 1$. Both the cubic

Received: November 25, 2011

Published: February 2, 2012

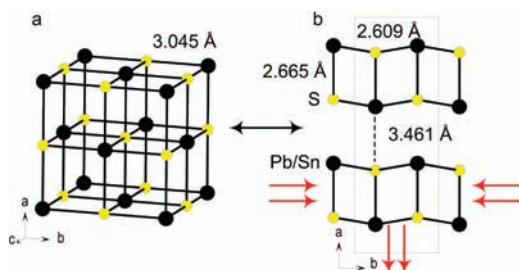


Figure 1. Cubic (a) and orthorhombic (b) crystal polymorphs of PbSnS_2 , showing the structural relationship through a compression along the b - c plane and an elongation along the a -axis (red arrows). The 3.045 Å distance is the average Pb/Sn-S bond length found in the cubic structure.¹⁶

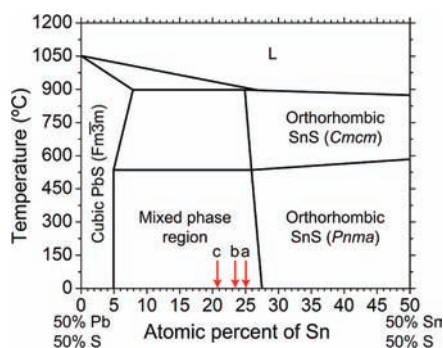


Figure 2. Schematic of the phase diagram of the PbS-SnS system. Labeled arrows (a), (b), and (c) show the compositions of the prepared $\text{Pb}_{2-x}\text{Sn}_x\text{S}_2$ nanocrystals.

and the orthorhombic structures are related through compression along the b - c plane, illustrated in Figure 1, where the thermodynamically more stable orthorhombic structure is denser. Therefore, the stabilization of cubic $\text{Pb}_{2-x}\text{Sn}_x\text{S}_2$ implies that a metastable kinetic phase (with respect to the bulk) is obtained because of low temperature synthesis or size reduction to the nanoscale. Similar phenomena are rare and have been observed in a few semiconductors where an unstable polytype is accessed on the nanoscale as for example in wurtzite-type MnSe (γ - MnSe),¹⁸ CuInS_2 ,¹⁹ CuInSe_2 ,²⁰ Cu_2SnSe_3 ,²¹ and $\text{Cu}_2\text{ZnSnS}_4$,²² orthorhombic-type MnAs ,²³ and tetragonal-type Ag_2Se (β - Ag_2Se).²⁴ The difference with the example we describe here is that the cubic structural form for the particular composition range reported for $\text{Pb}_{2-x}\text{Sn}_x\text{S}_2$ does not exist as the bulk form. To our knowledge the synthesis and properties of $\text{Pb}_{2-x}\text{Sn}_x\text{S}_2$ nanomaterials have not been reported. Here, we describe the cubic nanocrystals of $\text{Pb}_{2-x}\text{Sn}_x\text{S}_2$ prepared using a modified hot injection colloidal synthesis method. The stabilization of a new crystal form on the nanoscale for a composition which in the bulk adopts a different form (or does not even exist) is of fundamental interest in understanding the limits of phase stability as a function of size and in exploring the kinetics-thermodynamics balance. It is also an important new insight as to how new materials may be prepared that are unstable in the bulk but can be created uniquely on the nanoscale. In this regard the $\text{Pb}_{2-x}\text{Sn}_x\text{S}_2$ series in the cubic structure is a new class of nanomaterials.

EXPERIMENTAL SECTION

Materials. Trioctylphosphine (TOP, 90%), 1-octadecene (ODE, 90%), oleic acid (OA, 90%), oleylamine (OLA, 90%), lead acetate trihydrate, tin(II) acetate, anhydrous ethanol, hexane, carbon tetrachloride, acetone, and ethanol were purchased from Aldrich. Sulfur powder (99.999%) was purchased from 5N Plus. A 0.100 M sulfur precursor was prepared by dissolving 0.80 mmol (0.256 g) of sulfur in 8.00 mL of 1-octadecene at 100 °C for 2 h under a N_2 atmosphere. All other chemicals were used without further purification.

Synthesis of PbSnS_2 Nanocrystals. All syntheses were carried out under air-free conditions using a Schlenk line. In a typical synthesis, 0.400 mmol (0.152 g) of lead acetate, $\text{Pb}(\text{CH}_3\text{COO})_2 \cdot 3\text{H}_2\text{O}$, and 0.400 mmol (0.0947 g) of tin acetate $\text{Sn}(\text{CH}_3\text{COO})_2$, 8.00 mL of octadecene, 5.0 mL of oleic acid, and 5 mL of oleylamine were placed in a 100 mL Schlenk flask and dried under vacuum at 100 °C for 2–3 h with constant stirring to obtain a homogeneous pale yellow solution. The reaction flask was flushed with nitrogen, and the temperature was raised to 190 °C. At 190 °C, the prepared S precursor was swiftly injected. Upon injection, a dark brown colored mixture was observed. The temperature of the resulting mixture was maintained at 170–180 °C for 30, 60, or 120 s. The reaction was then cooled to room temperature using an ice-water bath. The resulting nanocrystals were precipitated by the addition of a solution of ethanol/hexanes (1:1) followed by centrifugation. Discarding the supernatant liquid gave a dark brown pellet of PbSnS_2 nanocrystals. The resulting nanocrystals were resuspended in hexanes and reprecipitated with excess ethanol. The purified nanocrystals can be dispersed in nonpolar organic solvents such as hexanes, chloroform, and carbon tetrachloride to form stable colloidal suspensions.

Characterization. An INEL CPS120 X-ray powder diffractometer with graphite monochromatized $\text{Cu K}\alpha$ radiation was used for powder X-ray diffraction (PXRD) measurements. Nanocrystal samples were deposited on a glass holder coated with a thin protective layer of grease, and the diffraction patterns were recorded at 40 kV and 20 mA operating conditions. Inductively coupled plasma-atomic emission spectroscopy (ICP-AES) measurements were carried out by dissolving nanocrystal powder in *aqua-regia* (HNO_3/HCl , 1:3 volumetric ratio) followed by dilution with ultrapure water. All samples were stirred with 0.500 M hydrazine in anhydrous acetonitrile at 25 °C for 2–3 days to remove the surfactants and vacuum-dried at 25 °C for 2 days before the analysis. The diffuse reflectance infrared spectrum was used to estimate the band gap of the materials by converting reflectance to absorption using the Kubelka-Munk function.²⁵

For the analysis of the local structure of the $\text{Pb}_{2-x}\text{Sn}_x\text{S}_2$ nanocrystals, powdered samples were packed in a glass capillary (1 mm diameter) under a N_2 atmosphere in a glovebox and flame-sealed. Diffraction data were collected at room temperature using the rapid acquisition pair distribution function (RA-PDF) technique²⁶ with a Perkin-Elmer α -Si detector and 58 keV energy X-rays ($\lambda = 0.2128$ Å) at the 11-ID-B beamline at APS. Accumulation of 150 frames with an exposure time of 1 s per frame was used to improve counting statistics. The data were integrated using the program FIT2D.²⁷ Various corrections were made to the data, such as subtraction of background and container, Compton and fluorescence scattering, geometric corrections, absorption, etc.²⁸ using the program PDFgetX2.²⁹ Simulations were carried out using PDFgui.³⁰

Transmission electron microscopy (TEM) analyses including EELS were conducted in dark field and bright field modes using a JEOL FasTEM 2100 HR TEM analytical electron microscope operating at an accelerating voltage of 200 kV. Samples for TEM analyses were prepared by depositing a drop of nanocrystal suspended in anhydrous hexanes onto the carbon-coated copper grids followed by solvent evaporation. The average particle sizes were obtained by visual measurements of the sizes of 100–200 individual nanoparticles observed in several TEM images. Elemental compositions, elemental maps, and spectral line profiles of the nanocrystals were obtained using dual *in situ* energy dispersive spectroscopy (EDS) units (Thermo

Scientific) attached to a Hitachi HD-2300 ultrahigh-resolution field emission scanning transmission electron microscope (STEM). For annealing studies nanocrystal powder samples were placed in an evacuated sealed quartz tube and annealed at different temperatures for different time periods.

RESULTS AND DISCUSSION

Synthesis and Structure of $\text{Pb}_{2-x}\text{Sn}_x\text{S}_2$ Nanocrystals.

Nanocrystals of $\text{Pb}_{2-x}\text{Sn}_x\text{S}_2$ were prepared using a modified hot injection method³¹ with oleic acid and oleylamine as surfactants and 1-octadecene as the reaction medium. This system of surfactants/solvent along with lead acetate as the lead precursor has been shown in the literature to be successful for the preparation of various lead chalcogenide nanocrystals with high stability, narrow dispersity, and cubic to spherical morphologies.^{11,32–34} Acetate salts of Pb^{2+} and Sn^{2+} were used as precursors, and elemental S was dissolved in 1-octadecene as the sulfur source. In the synthesis, the acetate salts of the precursors were converted into oleates upon heating the reaction mixture to 100 °C under vacuum for 2–3 h. This was signaled by the formation of a pale yellow solution. The temperature of the resulting solution was raised to 190 °C, and the prepared S precursor solution was swiftly injected. This temperature corresponds to the decomposition temperature of lead and tin oleates. SnCl_2 was also used as a Sn precursor; however very low Sn incorporation was observed in the prepared nanocrystals.

Powder X-ray diffraction (PXRD) patterns of the $\text{Pb}_{2-x}\text{Sn}_x\text{S}_2$ nanocrystals reveal the long-range crystalline nature of the particles with cubic rock salt symmetry ($Fm\bar{3}m$ space group), Figure 3. This result is in contrast with the bulk PbSnS_2 that

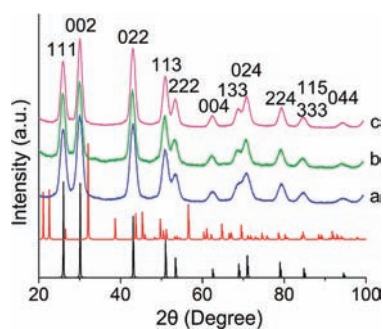


Figure 3. Powder X-ray diffraction pattern of the $\text{Pb}_{2-x}\text{Sn}_x\text{S}_2$ nanocrystals prepared at different lengths of reaction time: (a) 30 s, (b) 60 s, and (c) 120 s. Black lines represent the simulated PXRD pattern of bulk PbS (ICSD #657560). Red lines represent the simulated PXRD pattern of bulk PbSnS_2 (ICSD #156131).

normally crystallizes in an orthorhombic space group ($Pnma$). The diffraction patterns are shifted to larger 2θ values with respect to the powder pattern of pure cubic PbS suggesting a cell contraction consistent with the incorporation of Sn into the PbS lattice. The average particle sizes of the different samples were calculated based on the line broadening of the Bragg reflections and found to be in the range of 6.3–11.4 nm. No impurity Bragg peaks corresponding to SnS and/or the orthorhombic phase of PbSnS_2 ($Pnma$ space group) were observed in the diffraction patterns.

The average elemental compositions of the prepared particles were determined by energy dispersive spectroscopy in a scanning transmission electron microscope (STEM/EDS) and inductively coupled plasma-atomic emission spectroscopy

(ICP-AES). The results show the agreement of the values obtained from both analyses and are tabulated in Table 1.

Table 1. Elemental Composition, Average Particle Size, Lattice Parameters, and Optical Band Gaps of $\text{Pb}_{2-x}\text{Sn}_x\text{S}_2$ Nanocrystals

PbSnS ₂ Nanocrystals Samples	Elemental Compositions ^a	Value of x	Particle Size (nm)	Lattice Parameter (Å)	Band Gap (eV)
30 s	EDS: Pb _{1.04} SnS _{2.04}	0.97	PXRD: 6.3 ± 0.2	5.934(1)	0.57
	ICP: Pb _{1.03} SnS _{2.03}		TEM: 6.8 ± 0.5		
60 s	EDS: Pb _{1.11} SnS _{2.11}	0.87	PXRD: 10.7 ± 0.2	5.940(4)	0.54
	ICP: Pb _{1.13} SnS _{2.13}		TEM: 9.2 ± 0.5		
120 s	EDS: Pb _{1.37} SnS _{2.37}	0.60	PXRD: 11.4 ± 0.2	5.943(2)	0.52
	ICP: Pb _{1.40} SnS _{2.40}		TEM: 10.6 ± 0.6		

^aAverage compositions from three individual measurements.

Determination of the sulfur composition using both ICP-AES and STEM/EDS proved difficult since it is liberated as H_2S upon dissolving the nanocrystals in *aqua-regia* prior to ICP-AES analysis and the S $K\alpha$ line overlaps with the Pb $M\alpha$ line in the EDS analysis. Electron energy loss spectroscopy (EELS) was used to analyze the relative composition of S for each sample by comparing the ratio of Sn to S. The results verify the correct Sn to S ratio for each sample (Figure S1). It is interesting to note that as the growth time of nanocrystals is increased, they tend to be more lead rich. This is further supported by the expansion of the lattice parameter (Table 1) with increasing reaction time suggesting that over time the system tends to undergo equilibrium toward a more stable state by trying to purge Sn from the structure. Additional samples grown with much longer reaction times (240 and 360 s) were prepared to further investigate the extent of this effect. Consistently, these samples become even more lead rich as the Pb/Sn ratio approached almost 4:1 and 5:1 for the 240 and 360 s samples, respectively. This clearly demonstrates a strong tendency for the system to reduce the Sn “impurity” atoms from the cubic PbS rich sublattice. However, by controlling the kinetics of the reaction through rapid quenching, a metastable or a kinetically stabilized phase with a 1:1 Pb/Sn ratio can be obtained. Because of the decrease of the Sn fraction from the nanoparticles with reaction time we were not able to control the particle size for a given x composition of $\text{Pb}_{2-x}\text{Sn}_x\text{S}_2$.

Furthermore, we performed PDF analysis on the PbSnS_2 nanocrystals in order to verify that their short and medium range structure is indeed cubic and not locally distorted as in orthorhombic PbSnS_2 .^{35,36} It has been pointed out previously that it is possible for the long-range structure suggested by PXRD to be different from the short-range local structure and PDF analysis is key to resolving such issues.^{35,37,38} The experimental PDF plots and the corresponding fits of the cubic model of the $\text{Pb}_{2-x}\text{Sn}_x\text{S}_2$ nanocrystals prepared in 30, 60, and 120 s are shown in Figure 4. All three reaction conditions gave nanocrystals with the same cubic structure as indicated from the excellent agreement of the fits (red lines) with the experimental PDF data (black circles). The first observed interatomic vector in the experimental PDF at around 3 Å is characteristic of the M–S bond (M = Pb/Sn) in the rock salt

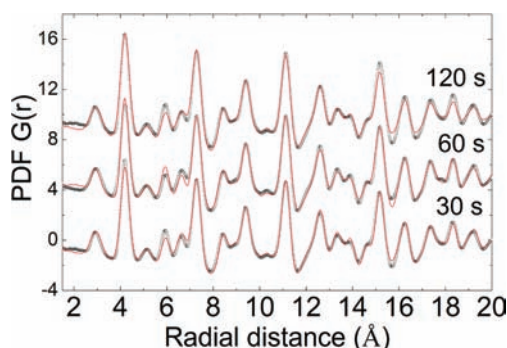


Figure 4. PDF plots of the $\text{Pb}_{2-x}\text{Sn}_x\text{S}_2$ nanocrystals prepared in 30, 60, and 120 s. Experimental data are shown in black circles, and the corresponding fits of the cubic NaCl-type model are shown in red lines. The fit of the cubic structure is in excellent agreement with the experimental data. The comparison of the fit of the orthorhombic model is shown in the Supporting Information (Figure S3).

structure while the corresponding M–S bonding distances in the distorted orthorhombic model are much shorter at ~ 2.61 and 2.66 Å (Figure 1).

Transmission electron microscopy (TEM) images of the PbSnS_2 nanocrystals without size-selective processing are shown in Figure 5a–c. The as-prepared nanocrystals are nearly

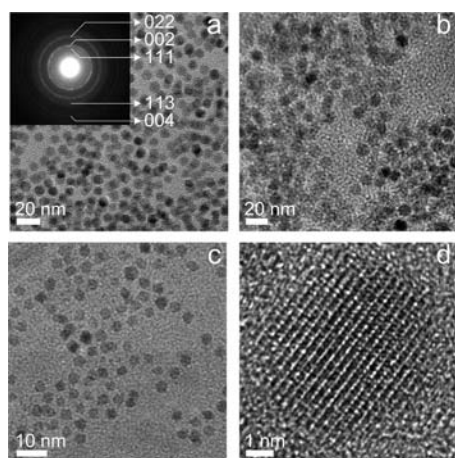


Figure 5. TEM images of the as-synthesized $\text{Pb}_{2-x}\text{Sn}_x\text{S}_2$ nanocrystals prepared at different reaction times: (a) 30 s, (b) 60 s, and (c) 120 s. Inset in (a) shows the selected area electron diffraction pattern from an ~ 200 nm \times 200 nm area of nanocrystals. The Bragg diffractions can be indexed to a cubic $Fm\bar{3}m$ space group. (d) HR-TEM micrograph of the 30 s sample ($x = 0.97$) shows a regular NaCl-type crystal structure viewed down the $[100]$ direction.

spherical in shape, and the average particle size ranges from 6.8 to 11.4 nm for different samples prepared at varying lengths of reaction time. Selected area electron diffraction (SAED) patterns collected from an ~ 200 nm \times 200 nm area of the 30 s sample (Figure 5a inset) clearly show that the Bragg diffractions correspond to the NaCl-structure type (Figure S2). The EDS spectral images recorded using scanning transmission electron microscopy (STEM) mode using a 1 nm scanning probe from the 60 s sample confirms the presence of all elements (Pb, Sn, and S) in a single nanocrystal (Figure 6b). The single phase homogeneity of the nanocrystals was further confirmed by the consistent rise and fall of Pb, Sn, and S signals moving from particle to particle shown in the EDS line scan

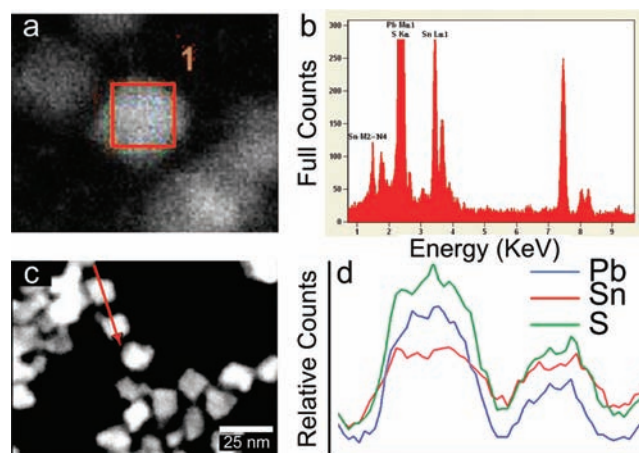


Figure 6. (a) STEM image of 60 s $\text{Pb}_{2-x}\text{Sn}_x\text{S}_2$ nanocrystal and (b) the corresponding EDS spectrum showing the presence of all the expected elements in a single nanoparticle. (c) STEM image of nanocrystals and (d) a line scan analysis through two individual particles (along direction of red arrow in (c)) confirming the homogeneous single phase behavior of the 60 s $\text{Pb}_{2-x}\text{Sn}_x\text{S}_2$ nanocrystals.

profile (Figure 6d). Similar results were obtained from the 30 and 120 s samples and demonstrate that nanoparticles prepared using this route are single phase and not phase-separated nanocrystals with localized PbS and SnS regions.

Energy Gaps and Electronic Structure. The synthesized $\text{Pb}_{2-x}\text{Sn}_x\text{S}_2$ nanocrystals exhibit well-defined band gap energies in the near-IR region (Figure 7). The band gap onset values in

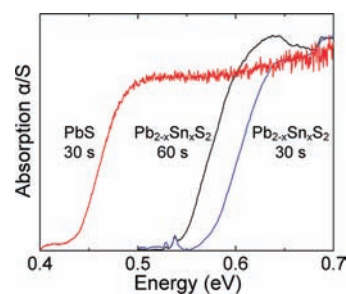


Figure 7. Near-IR absorption spectra of the 30 s (blue) and 60 s (black) $\text{Pb}_{2-x}\text{Sn}_x\text{S}_2$ and 30 s PbS (red) nanocrystals are shown. All samples were stirred in a 0.5 M hydrazine in acetonitrile solution for 2 d followed by vacuum drying; both steps prior to analysis were commenced at room temperature.

the range of 0.52–0.57 eV were estimated based on the electronic absorption spectra. The band gaps are higher than that of PbS nanocrystals of comparable size which is ~ 0.44 eV. These values are significantly different from the band gaps of bulk PbS, SnS, and PbSnS_2 , which are 0.37, 1.30, and 1.10 eV respectively.^{12,13}

Normally, the band gaps of a nanocrystalline semiconductor are blue-shifted compared to its bulk parent. In the case of $\text{Pb}_{2-x}\text{Sn}_x\text{S}_2$ nanocrystals the band gap is narrower than that of the bulk PbSnS_2 , and the reason for this is the different crystal structure of the latter. The proper comparison of band gaps is with the hypothetical cubic PbSnS_2 , which does not exist. Since the band gaps of the $\text{Pb}_{2-x}\text{Sn}_x\text{S}_2$ nanocrystals (0.52–0.57 eV) are expected to be blue-shifted by quantum confinement relative to bulk, we conclude that the band gap of the hypothetical cubic PbSnS_2 should be much narrower than the

0.52 eV of the nanocrystals and of course the 1.1 eV of orthorhombic PbSnS₂.

To gain insight into the band gap comparison of bulk cubic and orthorhombic PbSnS₂ we performed DFT electronic band structure calculations (using WIEN2k; see Supporting Information for details). The calculated band gap of the orthorhombic PbSnS₂ is 1.1 eV (Figure 8a) which is in good

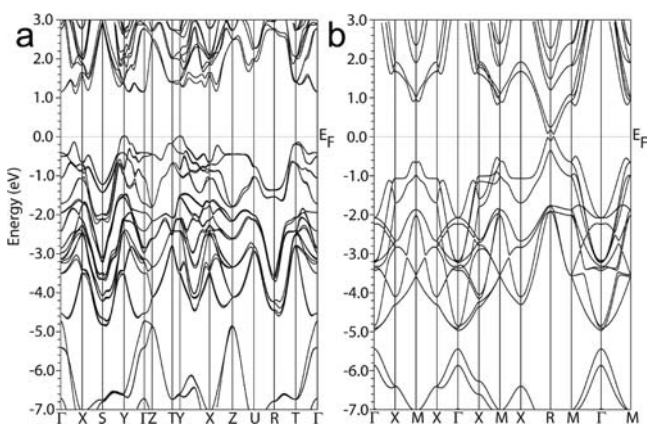


Figure 8. Electronic band structure near the Fermi level (E_F) for (a) orthorhombic PbSnS₂ and (b) cubic PbSnS₂. The difference in energy gaps between the two forms is dramatic.

agreement with the experimentally measured value.^{12,13} The calculated band gap of the hypothetical cubic PbSnS₂ is only 0.2 eV which is indeed much narrower than that of the orthorhombic form, Figure 8b. The density of states plots for both the orthorhombic and cubic structures suggest that the top of the valence band has mainly sulfur orbital character and the bottom of the conduction band is evenly occupied by p-states of Pb and Sn atoms. The lowering of the band gap originates from the extended three-dimensional connectivity in the cubic structure which gives rise to broader bands. The significantly larger energy gap of the orthorhombic structure is consistent with its greater thermodynamic stability and arises from the strong tendency of Sn²⁺ to stereochemically express its 4s lone pair of electrons. This tendency weakens in the corresponding Pb²⁺ ion.

Thermal Stability and Thermodynamic Phase Separation. In none of our synthetic procedures did we observe evidence of nanocrystals of PbSnS₂ in the orthorhombic structure. Therefore, we hypothesized that the cubic nanocrystals may be transformable to orthorhombic ones upon proper annealing treatment. However, this does not happen. Pb_{2-x}Sn_xS₂ nanocrystals ($x = 0.97$) annealed at 275 °C undergo sintering as evident from the growth of the crystallite size indicated in the PXRD patterns (Figure 9). Consequently, no transformation to the orthorhombic structure was observed, indicating the stability of the cubic particles up to this temperature. At higher temperatures (325–500 °C), however, the Pb_{2-x}Sn_xS₂ nanocrystals, which are solid solutions at room temperature, tend to phase-separate. At 325 °C the particles already show indications of phase separation in the PXRD patterns which show extra peaks corresponding to α -SnS. Samples annealed at 375 °C clearly exhibit phase separation into PbS and α -SnS which becomes complete between 400 and 500 °C, as all peaks in the PXRD pattern can be indexed to bulk PbS and α -SnS (Figure 9).

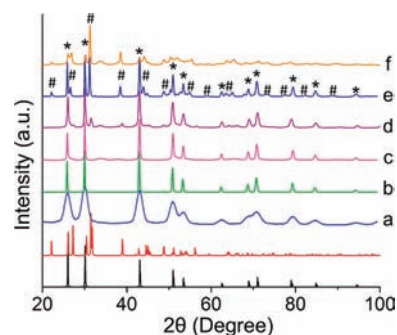


Figure 9. Powder X-ray diffraction patterns of the (a) Pb_{2-x}Sn_xS₂ (30 s) nanocrystals annealed at (b) 275, (c) 325, (d) 375, (e) 400, and (f) 500 °C for 4 h under vacuum. The diffraction peaks for pattern (d) are marked with * and # corresponding to PbS and α -SnS phases respectively. Black lines represent the simulated PXRD pattern of bulk PbS (ICSD #657560). Red lines represent the simulated PXRD pattern of bulk α -SnS (ICSD #156130).

CONCLUDING REMARKS

This study demonstrates the synthesis of semiconductor Pb_{2-x}Sn_xS₂ nanocrystals with a new cubic rock salt crystal structure and a composition range that is unstable in the bulk. The Pb_{2-x}Sn_xS₂ nanoparticles show absorption band onsets in the near-IR region which is consistent with size induced quantum confinement relative to a hypothetical bulk structure rather than the orthorhombic PbSnS₂ structure. The stabilization of the cubic NaCl-type structure is attributed to the influence of the nanoscale regime. One possible explanation could be the kinetic stabilization of the cubic structure under the rapid reaction conditions employed in the synthesis. However, given the fact that annealing of the nanocrystals below their decomposition point does not yield the orthorhombic PbSnS₂ structure implies that the stabilization may be thermodynamic in nature. Interestingly, the nanocrystals demonstrate a “self-cleaning mechanism” as the particles become more lead-rich as growth time is increased. This trend may arise from the well-known reluctance of the Sn²⁺ ion to adopt the perfect octahedral geometry, dictated by the NaCl structure. The Sn²⁺ ion in a sulfidic coordination environment strongly prefers a distorted geometry where the so-called inert lone pair of electrons is stereochemically expressed (as for example in the structures of bulk PbSnS₂ and SnS). The solution dispersible Pb_{2-x}Sn_xS₂ nanocrystals may be suitable for the deposition of thin films for various device applications. The implications of our results are broad since they point to new synthesis opportunities of novel nanocrystals with structures and compositions that are stable on the nanoscale but cannot exist as bulk crystals.

ASSOCIATED CONTENT

Supporting Information

EELS plots, indexed SAED pattern of Pb_{2-x}Sn_xS₂ nanocrystal, PDF fit of the orthorhombic model of PbSnS₂, and details of the DFT band calculation. This material is available free of charge via the Internet at <http://pubs.acs.org>.

AUTHOR INFORMATION

Corresponding Author

m-kanatzidis@northwestern.edu

Notes

The authors declare no competing financial interest.

■ ACKNOWLEDGMENTS

This research was supported by the Office of Naval Research (Grant N00014-10-1-0331). Electron microscopy and elemental analyses were performed at the Electron Probe Instrumentation Center (EPIC) facility of Northwestern University Atomic and Nanoscale Characterization Experimental (NUANCE) Center (supported by NSF-NSEC, NSF-MRSEC, KECK Foundation, and the State of Illinois) at Northwestern University. Use of the Advanced Photon Source, an Office of Science User Facility operated for the U.S. Department of Energy (DOE) Office of Science by Argonne National Laboratory, was supported by the U.S. DOE under Contract No. DE-AC02-06CH11357. R.B. Soriano is partly supported by the Hierarchical Material Cluster Program Fellowship at Northwestern University.

■ REFERENCES

- (1) Rogach, A. L.; Eychmuller, A.; Hickey, S. G.; Kershaw, S. V. *Small* **2007**, *3*, 536.
- (2) Luther, J. M.; Beard, M. C.; Song, Q.; Law, M.; Ellingson, R. J.; Nozik, A. J. *Nano Lett.* **2007**, *7*, 1779.
- (3) Schaller, R. D.; Sykora, M.; Jeong, S.; Klimov, V. I. *J. Phys. Chem. B* **2006**, *110*, 25332.
- (4) Talapin, D. V.; Murray, C. B. *Science* **2005**, *310*, 86.
- (5) Horikoshi, Y.; Tsang, W. T. *Semiconductors and Semimetals*; Academic: New York, 1985; Vol. 22.
- (6) Nimtz, G.; Schlicht, B. *Narrow-Gap Semiconductors*, Springer Tracts in Modern Physics; Springer Verlag: New York, 1985; Vol. 98.
- (7) Melngailis, I.; Harman, T. C. *Semiconductors and Semimetals*; Academic Press: New York, 1970; Vol. 5.
- (8) Johnsen, S.; He, J.; Androulakis, J.; Dravid, V. P.; Todorov, L.; Chung, D. Y.; Kanatzidis, M. G. *J. Am. Chem. Soc.* **2011**, *133*, 3460.
- (9) Schaller, R. D.; Sykora, M.; Pietryga, J. M.; Klimov, V. I. *Nano Lett.* **2006**, *6*, 424.
- (10) Ellingson, R. J.; Beard, M. C.; Johnson, J. C.; Yu, P.; Micic, O. I.; Nozik, A. J.; Shabaev, A.; Efros, A. L. *Nano Lett.* **2005**, *5*, 865.
- (11) Murphy, J. E.; Beard, M. C.; Norman, A. G.; Ahrenkiel, S. P.; Johnson, J. C.; Yu, P.; Micic, O. I.; Ellingson, R. J.; Nozik, A. J. *J. Am. Chem. Soc.* **2006**, *128*, 3241.
- (12) Thangaraju, B.; Kaliannan, P. *Cryst. Res. Technol.* **2000**, *35*, 71.
- (13) Unuchak, D. M.; Bente, K.; Kloess, G.; Schmitz, W.; Gremenok, V. F.; Ivanov, V. A.; Ukhov, V. *Phys. Status Solidi C* **2009**, *6* (5), 1191.
- (14) Hayashi, K.; Kitakaze, A.; Sugaki, A. *Mineral. Mag.* **2001**, *65*, 645.
- (15) Moh, G. H. *Mineral. Petrol.* **1987**, *36*, 191.
- (16) Mariano, A. N.; Chopra, K. L. *Appl. Phys. Lett.* **1967**, *10*, 3.
- (17) Lebedev, A. I.; Sluchinskaya, I. A.; Munro, I. H. *Fizika Tverdogo Tela* **2002**, *44*, 1568.
- (18) Sines, I. T.; Misra, R.; Schiffer, P.; Schaak, R. E. *Angew. Chem., Int. Ed.* **2010**, *49*, 4638.
- (19) Pan, D.; An, L.; Sun, Z.; Hou, W.; Yang, Y.; Yang, Z.; Lu, Y. *J. Am. Chem. Soc.* **2008**, *130*, 5620.
- (20) Norako, M. E.; Brutchey, R. L. *Chem. Mater.* **2010**, *22*, 1613.
- (21) Norako, M. E.; Greaney, M. J.; Brutchey, R. L. *J. Am. Chem. Soc.* **2012**, *134*, 23.
- (22) Lu, X.; Zhuang, Z.; Peng, Q.; Li, Y. *Chem. Commun.* **2011**, *47*, 3141.
- (23) Senevirathne, K.; Tackett, R.; Kharel, P. R.; Lawes, G.; Somaskandan, K.; Brock, S. L. *ACS Nano* **2009**, *3*, 1129.
- (24) (a) Ciucivara, A.; Sahu, B. R.; Kleinman, L. *Phys. Rev. B Condens. Matter Mater. Phys.* **2006**, *73*, 214105/1. (b) Karkamkar, A. J.; Kanatzidis, M. G. *J. Am. Chem. Soc.* **2006**, *128*, 6002.
- (25) (a) Liao, J. H.; Kanatzidis, M. G. *Chemistry of Materials* **1993**, *5*, 1561. (b) Chondroudis, K.; McCarthy, T. J.; Kanatzidis, M. G. *Inorganic Chemistry* **1996**, *35*, 840. (c) McCarthy, T. J.; Kanatzidis, M. G. *Chemistry of Materials* **1993**, *5*, 1061.
- (26) Chupas, P. J.; Qiu, X. Y.; Hanson, J. C.; Lee, P. L.; Grey, C. P.; Billinge, S. J. L. *J. Appl. Crystallogr.* **2003**, *36*, 1342.
- (27) Hammersley, A. P.; Svensson, S. O.; Hanfland, M.; Fitch, A. N.; Hausermann, D. *High Pressure Res.* **1996**, *14*, 235.
- (28) (a) Egami, T.; Billinge, S. J. L. *Underneath the Bragg peaks: structural analysis of complex materials*; Pergamon Press, Elsevier: Oxford, U.K., 2003. (b) Billinge, S. J. L.; Kanatzidis, M. G. *Chemical Communications* **2004**, 749. (c) Rangan, K. K.; Billinge, S. J. L.; Petkov, V.; Heising, J.; Kanatzidis, M. G. *Chemistry of Materials* **1999**, *11*, 2629.
- (29) Qiu, X.; Thompson, J. W.; Billinge, S. J. L. *J. Appl. Crystallogr.* **2004**, *37*, 678.
- (30) Farrow, C. L.; Juhas, P.; Liu, J. W.; Bryndin, D.; Bozin, E. S.; Bloch, J. P. T.; Billinge, S. J. L. *Condensed Matter* **2007**, *19*, 335219.
- (31) Murray, C. B.; Norris, D. J.; Bawendi, M. G. *J. Am. Chem. Soc.* **1993**, *115*, 8706.
- (32) Urban, J. J.; Talapin, D. V.; Shevchenko, E. V.; Murray, C. B. *J. Am. Chem. Soc.* **2006**, *128*, 3248.
- (33) Arachchige, I. U.; Wu, J.; Dravid, V. P.; Kanatzidis, M. G. *Adv. Mater.* **2008**, *20*, 3638.
- (34) Arachchige, I. U.; Kanatzidis, M. G. *Nano Lett.* **2009**, *9*, 1583.
- (35) Billinge, S. J. L.; Kanatzidis, M. G. *Chem. Commun.* **2004**, 749.
- (36) Masadeh, A. S.; Bozin, E. S.; Farrow, C. L.; Paglia, G.; Juhas, P.; Billinge, S. J. L.; Karkamkar, A.; Kanatzidis, M. G. *Phys. Rev. B* **2007**, *76*, 115413/1.
- (37) Arachchige, I. U.; Soriano, R.; Malliakas, C. D.; Ivanov, S. A.; Kanatzidis, M. G. *Adv. Funct. Mater.* **2011**, *21*, 2737.
- (38) Bozin, E. S.; Malliakas, C. D.; Souvatzis, P.; Proffen, T.; Spaldin, N. A.; Kanatzidis, M. G.; Billinge, S. J. *Science* **2010**, *330*, 1660.